

Future frame semantic segmentation of time-lapsed videos with large temporal displacement

Talha Siddiqui and Samarth Bharadwaj
IBM Research Labs, India

Abstract

An important aspect of video understanding is the ability to predict the evolution of its content in the future. This paper presents a future frame semantic segmentation technique to perform pixel-wise labeling of the current and future frames in a time-lapsed video. We specifically focus on time-lapsed videos with large temporal displacement to highlight the model’s ability to capture large motions in time. We first introduce a unique semantic segmentation prediction dataset with over *120,000* time-lapsed sky-video frames and all corresponding semantic masks captured over a span of five years in North America region. The dataset has immense practical value for cloud cover analysis, which are treated as non-rigid objects of interest. Next, our proposed recurrent network architecture departs from existing trend of using temporal convolutional networks (TCN) (or feed-forward networks), by explicitly learning an internal representations for the evolution of video content with time. Experimental evaluation shows an improvement of mean IoU over TCNs in the segmentation task by 10.8% for 10 mins (21% over 60 mins) ahead of time predictions. Further, our model simultaneously measures both the current and future solar irradiance from the same video frames with a normalized-MAE of 10.5% over two years. These results indicate that recurrent memory networks with attention mechanism are able to capture complex advective and diffused flow characteristic of dense fluids even with sparse temporal sampling and are more suitable for future frame prediction tasks for longer duration videos.

Introduction

To translate the significant progress made by the community in image semantic segmentation into better video understanding, memory networks are being employed to encode video content. Much like with humans, memory network allows systems to efficiently encode higher-order information content present in videos such as semantic structure across video frames. An interesting direction of research to enable deep neural networks in encoding this spatio-temporal semantic structure in videos is by future frame prediction (Luc et al. 2017; Mathieu, Couprie, and LeCun 2015; Srivastava, Mansimov, and Salakhudinov 2015). Pursing future frame prediction in videos allows us to build models that construct an internal representation of a video that captures the evolution of its content over time. Such a representation provides both pixel-level understanding that can be resolved

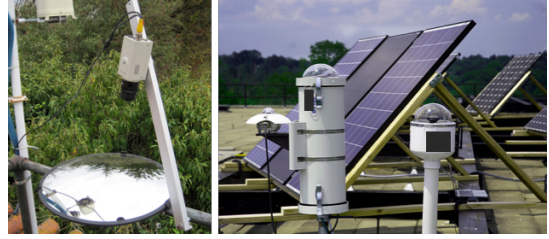


Figure 1: Time-lapsed videos of meteorological phenomenon captured for recreational and scientific observations. Estimating the likely future weather patterns from such time-lapsed videos can influence project planning leading to social and economical benefits.

to per-frame semantic segmentation, as well as frame-level property measurement, for both current and future frames.

This paper generalizes the problem of video future frame semantic segmentation prediction to time-lapsed videos with large temporal time-steps. Further, a secondary task of measurement of frame level properties related to the content of the video is used as an additional constraint. Our framework jointly learns the dual objective and additionally localizes the pixel level contribution of the measurement implicitly. Lastly, we show empirical results for the specific application of prediction of cloud region from time-lapsed sky-videos and measurement of solar irradiance.

Related Work

Semantic segmentation techniques for an image, or pixel-wise labeling from structure, have made large strides beginning with the fully-convolutional augmentation of convolutional networks (Long, Shelhamer, and Darrell 2015) and their variants with dilating or *a’trous* convolutions (Yu and Koltun 2015). In order to replicate similar success transitioning into video understanding, the computer vision community has embraced memory (recurrent) networks and more recently, temporal convolutional networks (TCN) (Bai, Kolter, and Koltun 2018) in various interesting ways.

We first position our work by briefly reviewing the recent flavours of memory networks to enhance video representations as follows:

Encoding short video sequences was initially viewed

as the next step to extending the performance of image understanding to videos. Early approach used two tier architectures (Karpathy et al. 2014) to compute features at different scales. Soon the encoder-decoder framework was favoured (Venugopalan et al. 2014) first by aggregation of frame representations and later with attention based approaches and 3D convolutional operations (Yao et al. 2015; Tran et al. 2015). (Klein, Wolf, and Afek 2015) present a dynamic convolution approach to predict short term weather from radar imaging sequences. However, a sufficiently robust representation of video frames becomes challenging with increasing length and complexity in context. (Vondrick, Pirsivash, and Torralba 2015) approach anticipating the likely-labels in the future frames without flow.

Unsupervised next frame prediction was introduced by (Srivastava, Mansimov, and Salakhudinov 2015), which provides video representations using LSTMs in the encoder-decoder framework. The reconstruction error is minimized in a composite encoder-decoder model that simultaneously predicts now and future frames. (Shi et al. 2015) extend the framework by introducing spatially constrained or convolutional LSTMs. The authors view the memory units as hidden layers and convert the input-state transition to convolution operations. These operations induce spatial structure in the memory units that is lacking in LSTM and can help encode evolving content in videos. Recently, (Hou and Wu 2018) utilize mid-level video frame encodings to capture semantic concepts in action recognition.

Flow estimation that is based on recurrent networks is implicitly computed and often intertwined with next frame prediction. Video encoder-decoder performance may improve with an additional penalty, added to the overall loss, of gradient smoothness parameters (Patraucean, Handa, and Cipolla 2015). Explicit optical flow approaches (Weinzaepfel et al. 2013; Ilg et al. 2016; Feichtenhofer, Pinz, and Zisserman 2016; Hur and Roth 2017) compute dense flow vectors for video understanding that track the motion of every pixel in the image. Such approaches are also shown to improve related tasks such as occlusion detection when exploited jointly. (Feichtenhofer, Pinz, and Zisserman 2017) use the model architectures of explicit flow, two consecutive frames as simultaneous inputs, to improve both tracking and object detection in videos.

Recurrent attention is an aspect of semantic segmentation which identifies individual instances of class. While the approaches presented in literature are evaluated on images, they use memory networks for sequentially predicting objects. Graphical models have been replaced in favour of recurrent networks with attention feedback, termed recurrent attention. (Romera-Paredes and Torr 2016) use a convolutional LSTM (ConvLSTM), while (Ren and Zemel 2016) later relax the spatial constraint for instance segmentation to capture disconnected instances of a given semantic class. Recently, (Piergiovanni, Fan, and Ryoo 2017) use temporal attention filters to identify latent sub-events in videos.

Temporal convolutional networks (TCN) (Bai, Kolter, and Koltun 2018) refer to convolutional network architecture that are utilized for temporal prediction tasks such as next frame prediction. Unsupervised reconstruction of

videos produces next frames but with noise and blurring, (Mathieu, Couprie, and LeCun 2015) replace the squared error loss with adversarial training method and show improvement in reconstruction. (Luc et al. 2016) first propose using adversarial training for semantic segmentation. They next extend the work (Luc et al. 2017) to propose future frame and semantic segmentation prediction in the context automatic driving problem. Their approach uses convolutional filters with auto-regression for very short term forecasting of future semantic masks. While the approach has shown excellent results on the Cityscapes dataset (Cordts et al. 2016), the prediction task in the dataset is limited to 0.5 seconds future prediction. This may have limited practical use in automated driving applications. (Jin et al. 2017a) propose video scene parsing by using predictive feature learning and prediction steering parsing. Their predictive feature learning architecture learns to extract spatiotemporal features by enforcing the model to predict a future frame in the sequence. They extend their work (Jin et al. 2017b) and propose simultaneous scene parsing and optical flow for future video frames. They state that capturing motion dynamics as well as predicting semantic masks are correlated problems and benefit from each other. However to the best of our knowledge, there is no recent work which illustrates the performance of spatiotemporal memory networks aided with spatial attention in predicting future frame semantic masks. Recently, (Miller and Hardt 2018) argue that the comparable performance of recurrent networks can often be achieved simply with feed-forward networks in an auto-regression fashion. Here, we show the merit of memory networks over auto-regression in time-lapsed videos with large temporal displacement.

Key Contributions

The key contributions of this research can be summarized as follows:

- We propose a novel future semantic mask prediction framework for simultaneously performing two collegial tasks, namely *segment* and *measure* that often occur together in various applications of video understanding.
- We propose a memory network based approach for future frame segmentation in time-lapsed videos of weather phenomenon. We show that the performance of memory networks can be considerably amplified with spatial attention models and a dual objective.
- The time-lapsed Sky-video dataset introduced in this paper represents, in our view, a stronger challenge to the semantic segmentation prediction problem by relaxing two assumptions, object rigidity and temporal continuity. The dataset contains clouds at a frame rate of 6 frames per hour.
- Our proposed approach out-performs state-of-art semantic pixel-wise labeling approaches that are designed for short-term videos on the sky-video dataset. The result makes a case for ConvLSTMs with attention as a middle ground between unsupervised recurrent nets and temporal convolutional feed-forward networks.

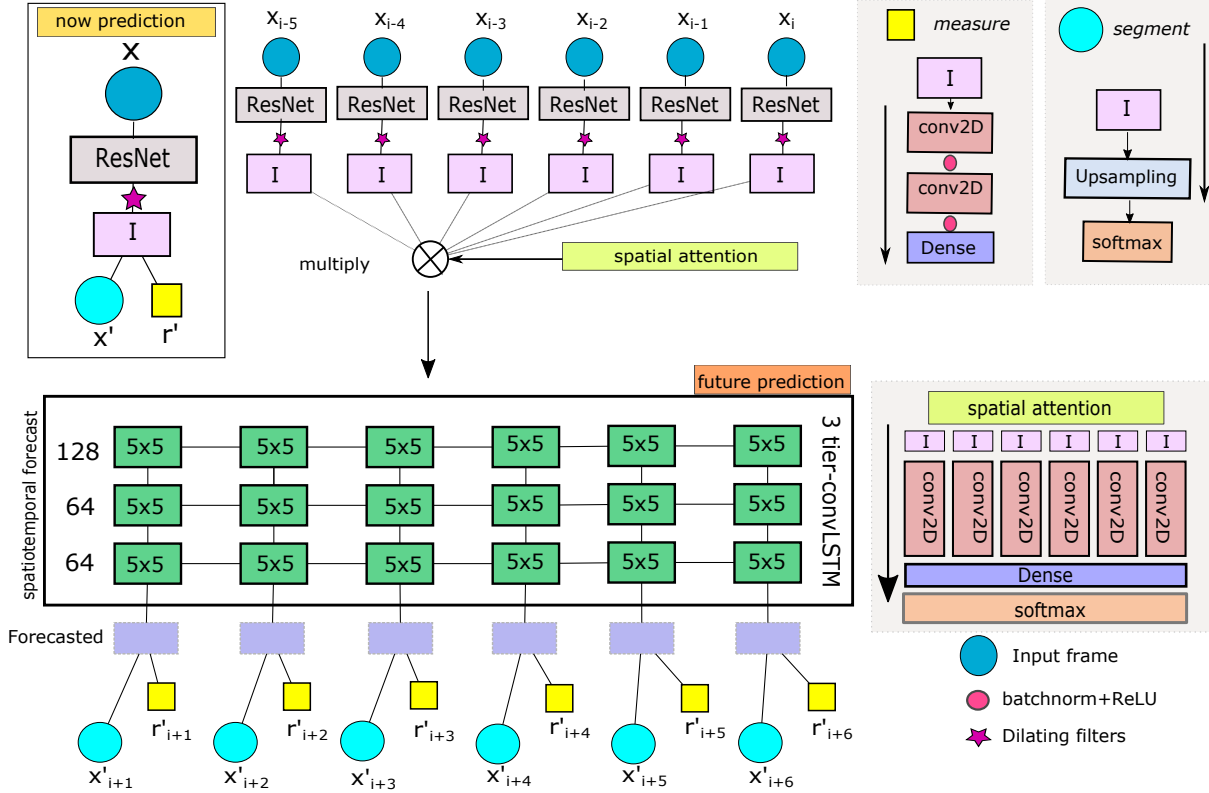


Figure 2: [Best viewed in colour] The proposed *future* video frame semantic segmentation approach explained here. For each video frame (x), a representation tensor (I) is obtained using ResNet with dilating filters. I is used in the *now* model to predict both the current semantic mask (x'), with convolutions, batchnorm+ReLU. The *future* model is a 3-tier ConvLSTM over the frame representations I of the previous n frames. Further, spatial attention is applied on the frame representations to further enhance performance. (Details in Section Model).

Model

We present a *future* video-frame semantic segmentation approach designed for time-lapse videos of weather phenomenon. The proposed end-to-end trainable approach performs two tasks: *segment* provides a semantic segmentation (or pixel-wise labeling) of the objects of interest in a current or future frames, and, *measure* regresses and also forecasts a frame-level property related to the content of the video. Problems in recent literature, such as object detection and semantic segmentation prediction in videos (Luc et al. 2017), partial object counting (Seguí, Pujol, and Vitria 2015; Chattopadhyay et al. 2016), and video question answering ((Zeng et al. 2017)) can be viewed within our framework.

We first describe the architecture of the model followed by our utilization of the spatial attention models to enhance the future prediction. We further describe the co-dependency in the architecture of the *segment* and *measure* components and argue that our architecture choice enables a spatially constrained representation to encode *partial*-contributions of the measured property from all localized regions of a given video frame.

Notations

Notationally, given a video $V \in \mathbb{R}^{N \times W \times H \times 3}$ which contains N frames, $V^{1:N}$ with frames $\{x_1, x_2, x_3, \dots, x_N\}$, we propose a framework to determine a model (\mathcal{M}^θ and \mathcal{M}^{θ_c}), that produces both frame-wise semantic segmentation of c classes of interest and their corresponding measurements, given by $\hat{V}_{\mathcal{M}^\theta}^{1:t} = \{(x'_1, r'_1), (x'_2, r'_2), (x'_3, r'_3), \dots, (x'_t, r'_t)\}$, where $x' \in \mathbb{R}^{W \times H \times c}$, and $r' \in \mathbb{R}$ is a scalar predicted value per frame. The *now* and *future* predictions for a look-back period t are respectively obtained as follows:

$$\begin{aligned} (x', r') &= \mathcal{M}^\theta(x) \\ \hat{V}^{i:i+t} &= \mathcal{M}^{\theta_c}(V^{i-t:i}) \end{aligned} \quad (1)$$

The *future* model (\mathcal{M}^{θ_c}) is built over an intermediary representation of an input video frame I_i obtained from the *now* model \mathcal{M}^θ . Further, the model is learnt over a training set for V with ground truth semantic segmentation $S \in \mathbb{R}^{N \times W \times H \times c}$, containing $\{y_1, y_2, y_3, \dots, y_N\}$, and the scale property measurement given by $\{m_1, m_2, m_3, \dots, m_N\}$.

Architecture

An overview of the proposed architecture for *segment* and *measure* for both *now* and *future* video frames prediction is illustrated in Fig. 2. We describe important details of the architecture that are relevant to the analysis, deferring remaining details of the model, such as parameters of layers, to the Supplementary.

Now model: Our approach utilizes the ResNet50 (He et al. 2016) as the front-end model. We further augment the last convolutional layer with dilation (Yu and Koltun 2015), to obtain the fully convolutional layer (*fc7*) that is used as a representation vector (I). Dilated convolutions are used to capture features at multi-scales without adding additional layers. All convolutional blocks are interlaced with Batch-norm and *ReLU* non-linearity and use bi-linear up-sampling to merge the skip-connections.

The representational vector (I) obtained from the front-end model is bifurcated into the *segment* branch, that is upsampled to the semantic segmentation mask resolution. Pixel label assignment is performed with *softmax*. Conversely, the *measure* branch is up-sampled with convolution up-sampling layers, again interlaced with Batch-norm and *ReLU* non-linearity. The prediction measure is aggregated over a dense connection, with dropout, to a single value.

Future model: To perform future frame prediction, we use a recurrent architecture to predict tensor I_i by utilizing only the corresponding representation tensors.¹ ($\{I_{i-t}, \dots, I_i\}$) from historical frames. In order to preserve the *spatial correspondence* of the *fc7* representation, we utilize convolutional LSTMs (ConvLSTM) (Shi et al. 2015) that contain memory gates which are convolutional operations and preserve the spatial and temporal structure while inducing memory into the architecture.

Specifically, multiple tiers of ConvLSTM are used over a look-back period t , to construct the representations ($\{I_i, \dots, I_{i+t}\}$). We also observe that the performance of the stacked ConvLSTMs is significantly improved with the addition of spatial attention mechanisms, described next.

Future prediction with spatial *soft*-Attention

Our architecture uses stacked convolutional LSTMs to predict semantic representations of the future frames, from a look back period t , given by $\mathbb{I}=\{I_{i-t}, \dots, I_i\}$. Attention is computed over the spatial, temporal and class label (c) dimensions of I to induce more structure in the predictions, that can particularly be affected by the large temporal displacements in time-lapsed videos.

Spatial attention is assigned to a given pixel (i, j) of \mathbb{I} over all the values in the look back period t , of the given and neighbourhood pixels (p), with a simple convolutional operation. This can be described as:

$$A_{(i,j)} = \mathbb{I}(i, j) \otimes h(p, p) \quad (2)$$

where h is an additional set of convolutional filters learnt in the overall architecture. The filters are oversampled and

¹we use the term tensors rather than vectors to indicate their multi-dimensional nature.

reduced with a densely connected operation to obtain the attention mask A . The mask obtained is further normalized with *softmax* and multiplied with the original samples \mathbb{I} . This attention model utilizes learned convolutional operations over the *entire* training batch matrix, learning attention without explicit temporal structure or memory. We also compute *softmax* attention (Olah and Carter 2016) over \mathbb{I} averaged over all the pixels and use for baseline comparison, that we term *mean* attention.

Loss

As shown in the Fig. 2, the model’s end-to-end trainable architecture performs both semantic segmentation prediction and measure prediction for both *now* and *future* problem. The loss function is a weighted mixture of the loss from each task, given in Eq. 3:

$$L_w(x, x', r, r') = \lambda(CL_{\gamma,\alpha}(x, x')) + (\mathcal{H}(r, r')) \quad (3)$$

where $CL_{\gamma,\alpha}$ is the combined loss given in Eq. 4, and the λ is the normalizing weight to equally favour predictions of segment and measure respectively.

$$CL_{\gamma}(x, x') := FL_{\gamma,\alpha}(x, x') + CE(x, x') \quad (4)$$

$$FL_{\gamma,\alpha}(x, x') := -\alpha x^\gamma \log(x') + (1-x)^\gamma \log(1-x') \quad (5)$$

The combined loss is a combination of focal loss ($FL_{\gamma,\alpha}$) (Lin et al. 2017) and categorical cross-entropy (CE) measured for the semantic segmentation over every pixel. The focal loss is given by Eq. 5 with tuneable parameters set to control the order of magnitude ($\gamma = 2$ and $\alpha = 0.5$). The combined loss penalizes incorrect classification of pixel semantic label, with larger focus on harder predictions, such as cloud pixels. We observe small improvement in segmentation compared to pixel-wise categorical cross entropy.

$$\mathcal{H}(r, \hat{r}) := \log(m * \cosh(r - \hat{r})) \quad (6)$$

To compute prediction errors of the frame level measurement, in this case the irradiance forecast, smooth Huber loss is used (Eq. 6). We prefer the hyperbolic version for the smoothness, which is magnified at $m = 100$. Empirically, irradiance prediction below $100 W/m^2$ are less important.

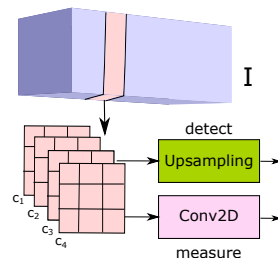


Figure 3: An illustration of the bifurcation point of the model. Note I is a tensor spatially consistent with the image rather than a flat vector.

Segment with partial Measure

A unique feature of our architecture is the strong constraint for every spatial region to have a *partial*-contribution to the measured property r . As illustrated in Fig. 3, the bifurcation point of the architecture that branches into two tasks, *segment* and *measure*, emerge from a single down-sampled representation I (rather than a flat vector), which is received directly from the input image for *now* prediction, and is predicted from the stacked convolutional-LSTMs for the *future* prediction. In either case, for a given pixel, the *segment* branch up samples I using *only* local neighbourhood vectors. Similarly, for the *measure* branch, the convolution filters again operate only on the local neighbourhood of the pixel to predict r . Extending this intuition to the *future* prediction model, the stacked convolutional LSTMs are also constraint locally to predict the representation I for a future frame. Hence, we assert that our framework implicitly generates the *partial*-contribution of the measure property over the spatial region of the image. Hence, measure is an integral over a downsampled semantic mask prediction.

Evaluation

In this section, we describe the performance of the proposed approach on newly introduced sky-video dataset. The proposed approach is compared on the same parameters and protocol with two different attention mechanisms and with a temporal convolutional network (Luc et al. 2017) designed for shorter videos. The baseline persistence model refers to a model which simply uses the predicted semantic mask of the current frame (at t) as the semantic mask of the future frame.

Sky-video dataset and protocol

A sky-video is obtained from an upward facing wide-angle lensed video camera such as the one shown in Fig. 1. The dataset is recorded at Solar Radiation Research Laboratory (SRRL), Golden, Colorado (Andreas 1981)², situated in North America. The time-lapsed videos are recorded using a commercial sky imager (TSI) (Morris 2005) at every 10 minutes interval. A mechanical sun tracker is used to block the sun preventing saturation in the image and blooming effects. The dataset is available for the last 13 years from 2005-2017. Over the same period, we obtained solar irradiance measurements (in W/m^2) from the same location using a pyranometer. The cloud cover, defined as the ratio of pixels labeled cloud in the sky image is correlated with irradiance measure (0.67 on the training set). More details of capture device and sample frames illustrations are in Supplementary. We showcase our experiments on the images captured in the year 2010-2014 with the total number of 123,064 images in our dataset. The input video consists of RGB frames of dimensions $W = 320, H = 320$. The TSI imager also provides ground truth segmentation masks of four classes in the sky, namely, *sky*, *cloud*, *sun*, and *tracker* ($c = 4$). We use data from 2010-2012 in training (73,120 images) and from

²the dataset is available for download at www.nrel.gov/midc/srsl_bms/. The processed dataset is available for easy reproducibility at <https://bit.ly/2Bw7HGP>.

Table 1: normalized-MAE of Irradiance (W/m^2) (%) and IoU for segmentation in Now prediction on the test set

Experiment	n-MAE	IoU Cloud	IoU Sky
Baseline (only Irradiance)	11.31	-	-
ResNet50 + dilation	10.96	83.31	87.89

2013-2014 (49,944 images) for testing based on availability and quality of ground truth.

For the *future* model, we use look-back (t)=1hour (or six samples at 10mins interval) and batch-size=4 (3046 batches per epoch) and compute a forward prediction for the same size. We start with a learning rate of 0.002 and reduce with power decay ($\gamma = 0.9$) per epoch. A weight decay of 0.00005 with l_2 -norm regularizer is used for all convolutional layers. *Adam* optimizer is used for all our experiments. We report pixel-level segmentation accuracy, Intersection over Union (IoU) and normalized mean absolute error (nMAE) as applicable.

Table 2: Measure Task: normalized-MAE (%) of Irradiance (in W/m^2) for Future using proposed Attention Mechanisms on Testing Data

Attention Mechanism	+10 mins	+20 mins	+30 mins
Without	28.057	28.472	28.229
(Olah and Carter 2016)	21.853	22.954	24.013
Spatial	19.486	22.051	23.472
Attention Mechanism	+40 mins	+50 mins	+60 mins
Without	27.526	27.872	27.883
(Olah and Carter 2016)	25.048	26.210	27.173
Spatial	24.934	25.982	26.938

Analysis

The performance of the *now* prediction model in Table 1 shows that the ResNet50 model (with dilated convolutional filters) captures cloud region with Intersection over Union (IoU) of 83.31% and IoU of 87.89% on sky with the *segment* task on sky-video frames. Simultaneously, the model has a normalized mean absolute error (nMAE) of 10.96% on the *measure* task of solar irradiance. The total accuracy measure which includes the segmentation accuracy of the tracker and boundary bezel of the frame is 94.57%. As shown in Fig. 4, the ground truth masks are grainy pixel segmentation, whereas our model generates semantic masks by linear up-sampling from a low dimensional representation, resulting in smoother segmentation masks.

Fig. 4 also illustrates sample image frames and their corresponding segmentation masks obtained. Unlike rigid objects in benchmark vision datasets, clouds exhibit non-compressible fluid behaviour such as advection and diffusion. The trained *now* prediction model weights are also used as pre-training initialization weights in the *future* prediction experiments. As shown in the *now* experiments in Table 1, our approach out-performs a direct regression model, trained separately with the loss function corresponding to only *measure*, Eq. 6. We exclude a comparison of exist-

Table 3: Segment Task: Accuracy(%) and IoU for Future Frames using various Attention Mechanism on Testing Data

Attention Mechanism	Accuracy	+10 mins		+20 mins		+30 mins	
		Cloud	Sky	Cloud	Sky	Cloud	Sky
Persistence	80.55	64.04	69.77	59.31	65.65	55.97	62.74
Without	87.59	61.61	69.76	61.36	69.57	61.15	69.55
Mean (Olah and Carter 2016)	89.00	70.39	77.25	68.39	75.34	66.15	73.38
Spatial	89.38	74.15	79.57	70.48	76.43	67.73	73.81
(Luc et al. 2017)	75.94	63.15	68.88	58.08	64.08	52.64	56.72
Attention Mechanism	Accuracy	+40 mins		+50 mins		+60 mins	
		Cloud	Sky	Cloud	Sky	Cloud	Sky
Persistence	80.55	53.14	60.31	50.14	57.90	47.05	55.77
Without	87.59	60.97	69.49	59.71	69.11	58.66	69.53
Mean (Olah and Carter 2016)	89.00	63.89	71.75	60.96	70.13	58.87	69.65
Spatial	89.38	65.29	71.71	62.49	69.89	60.16	69.05
(Luc et al. 2017)	75.94	48.02	49.61	43.76	42.89	39.55	35.53

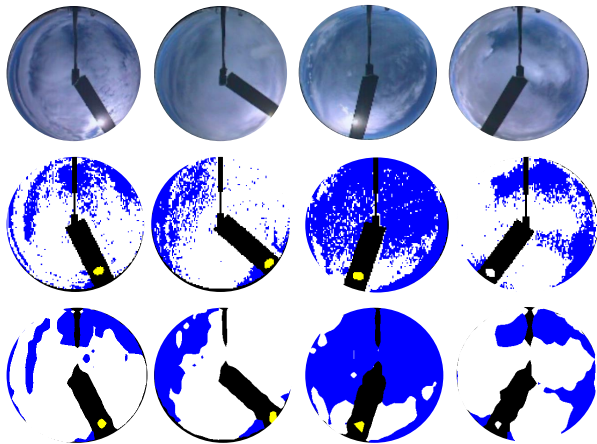


Figure 4: Sample semantic segmentation of *now* predictions. The three rows in the illustration are a sequence of input frames, the corresponding ground truth and semantic masks, respectively.

ing literature in skycamera based irradiance measurement, as all deep neural network models far-outperform previous approaches when trained with data from the same location (Paoli et al. 2010). The measure task from the *future* prediction model forecasts the solar irradiance for next hour at 10 minutes interval. The performance of the model is improved by spatial attention mechanism. Specifically, the normalized-MAE% for 10 minutes forecast of solar irradiance improves from 28.1% without attention, and 21.8% for mean attention, to 19.5% for spatial attention.

The *segment* task in *future* prediction model forecasts semantic segmentation masks for the next hour at 10 minutes interval. For 10 minutes ahead-of-time prediction, the IoU for cloud segmentation is improved from 61.6% (with no attention) to 74.2% with spatial attention. Similar improvement from 61.2% to 67.7% is observed for 30 minutes

ahead-of-time predictions. In order to maximize the effect of attention mechanisms, we compute the attention vector only on the $c = \text{cloud}$ dimension. We find empirically that this improves the affect of attention in the *future* prediction models. We choose the *cloud* class, as it is of most value in this application scenario.

Fig. 5(a) represents a one hour temporal frames (V) that is input to the model, the *expected* segmentation masks (S), and the true original future frames (\hat{V}) for the next one hour prediction. Frames at intervals $t - 50, t - 40, t - 30, t - 20, t - 10, t$ are used to generate the semantic segmentation masks for intervals $t + 10, t + 20, t + 30, t + 40, t + 50$ and $t + 60$ minutes. Fig. 5(b) represents *corresponding* semantic segmentation masks as generated by various attention mechanisms for one hour ahead sky orientation. The first row represents predicted semantic masks without the aid of any attention. Masks predicted for later intervals using this model are not accurate and mis-classify many cloud regions as sky. The next two rows represent semantic masks generated using mean, and spatial attention respectively. It can be inferred that masks generated using spatial attention attend to a more precise representation of sky and hence generate better frames even for the later time intervals.

An empirical analysis of the *partial*-contribution from localized regions of the video frame for the total estimate of solar irradiance requires pixel level ground truth for solar irradiance. However, to our knowledge, such an instrumentation is not available. As discussed above, our architecture design ensures that both *segment* semantic mask of sky region and *measure* of solar irradiance are upsampling estimates from a single $I(fc7)$ tensor of course resolution. We assert that the model implicitly localizes the individual contributions of each sky pixel to obtain the total measurement.

Comparison with (Luc et al. 2017): We use the open-source implementation provided by the authors for this comparison. The base model (pre-trained ResNet with dilated convolution layers) is the same as the proposed model but computed at two scales as per their algorithm (Mathieu, Couprie, and LeCun 2015). The summation of L_1 loss with

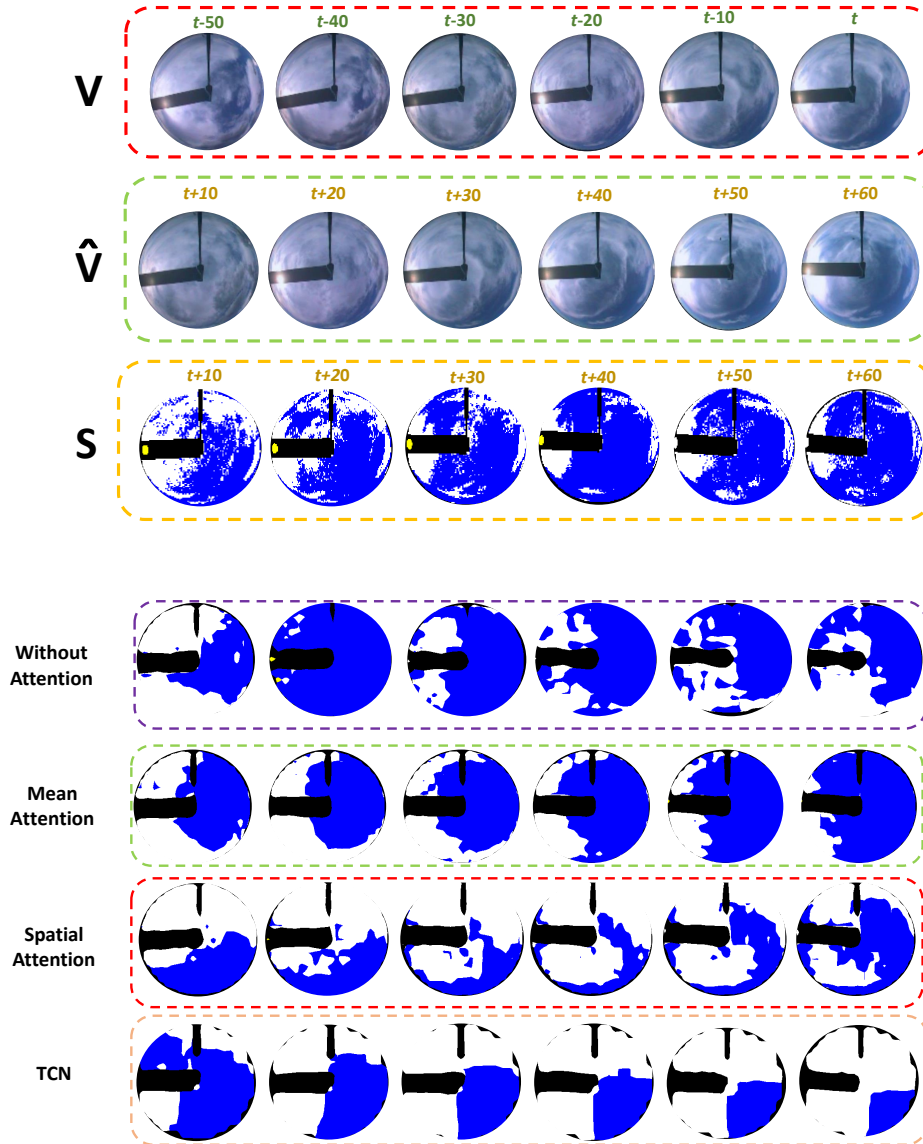


Figure 5: Performance of *segment* task on 6 consecutive frames of one hour. The figure contains input (V), target (\hat{V}), ground truth (S) and 6 predictions (next 1 hour) for multiple attention methods and TCN (Luc et al. 2017).

gradient difference loss using Adam optimizer. As shown in Table 3, the IoU for the first future frame prediction (+10 minutes ahead) is 63.15%, which is comparable to the persistence model. However, the performance degrades by the third frame (+30 minutes ahead) to 52.65% and by the sixth frame (+60 minutes) to 39.55% due to the compounding effects of the auto-regression approach. The bottom row of Fig. 5(b) illustrates the effect of compounding errors.

Conclusion

We uniquely evaluate our future frame prediction for video understanding on a time-lapse videos of the sky. Our approach outperforms temporal CNNs at future pixel-wise la-

beling of sky regions. Further, the integral over the spatial regions of the image can produce an estimate of the total solar irradiance from the sky. The solar irradiance prediction so obtained closely approximate a pyranometer readings over two years test period without re-training or online update, indicating the efficacy of the frame representation. Further, the architecture compel the model to learn localized partial-contributions of solar irradiance from different regions of the sky. All scripts will be open-sourced for easy reproducibility (<https://bit.ly/2Bw7HGP>).

References

Andreas, A.; Stoffel, T. 1981. Nrel solar radiation research laboratory (srrl): Baseline measurement system (bms).

- Bai, S.; Kolter, J. Z.; and Koltun, V. 2018. An empirical evaluation of generic convolutional and recurrent networks for sequence modeling. *arXiv preprint arXiv:1803.01271*.
- Chattopadhyay, P.; Vedantam, R.; RS, R.; Batra, D.; and Parikh, D. 2016. Counting everyday objects in everyday scenes. *arXiv preprint arXiv:1604.03505*.
- Cordts, M.; Omran, M.; Ramos, S.; Rehfeld, T.; Enzweiler, M.; Benenson, R.; Franke, U.; Roth, S.; and Schiele, B. 2016. The cityscapes dataset for semantic urban scene understanding. In *Proc. of the IEEE Conference on Computer Vision and Pattern Recognition (CVPR)*.
- Feichtenhofer, C.; Pinz, A.; and Zisserman, A. 2016. Convolutional two-stream network fusion for video action recognition. In *Proceedings of the IEEE Conference on Computer Vision and Pattern Recognition*.
- Feichtenhofer, C.; Pinz, A.; and Zisserman, A. 2017. Detect to track and track to detect. *arXiv preprint arXiv:1710.03958*.
- He, K.; Zhang, X.; Ren, S.; and Sun, J. 2016. Deep residual learning for image recognition. In *Proceedings of the IEEE Conference on Computer Vision and Pattern Recognition*.
- Hou, J., and Wu, X. 2018. Unsupervised deep learning of mid-level video representation for action recognition. *Thirty-Second AAAI Conference on Artificial Intelligence*.
- Hur, J., and Roth, S. 2017. Mirrorflow: Exploiting symmetries in joint optical flow and occlusion estimation. In *Proceedings of International Conference on Computer Vision*.
- Ilg, E.; Mayer, N.; Saikia, T.; Keuper, M.; Dosovitskiy, A.; and Brox, T. 2016. Flownet 2.0: Evolution of optical flow estimation with deep networks. *arXiv preprint arXiv:1612.01925*.
- Jin, X.; Li, X.; Xiao, H.; Shen, X.; Lin, Z.; Yang, J.; Chen, Y.; Dong, J.; Liu, L.; Jie, Z.; Feng, J.; and Yan, S. 2017a. Video scene parsing with predictive feature learning. In *2017 IEEE International Conference on Computer Vision (ICCV)*, 5581–5589.
- Jin, X.; Xiao, H.; Shen, X.; Yang, J.; Lin, Z.; Chen, Y.; Jie, Z.; Feng, J.; and Yan, S. 2017b. Predicting scene parsing and motion dynamics in the future. In Guyon, I.; Luxburg, U. V.; Bengio, S.; Wallach, H.; Fergus, R.; Vishwanathan, S.; and Garnett, R., eds., *Advances in Neural Information Processing Systems 30*. Curran Associates, Inc. 6915–6924.
- Karpathy, A.; Toderici, G.; Shetty, S.; Leung, T.; Sukthankar, R.; and Fei-Fei, L. 2014. Large-scale video classification with convolutional neural networks. In *Proceedings of the IEEE conference on Computer Vision and Pattern Recognition*.
- Klein, B.; Wolf, L.; and Afek, Y. 2015. A dynamic convolutional layer for short range weather prediction. In *Proceedings of the IEEE Conference on Computer Vision and Pattern Recognition*.
- Lin, T.-Y.; Goyal, P.; Girshick, R.; He, K.; and Dollár, P. 2017. Focal loss for dense object detection. *arXiv preprint arXiv:1708.02002*.
- Long, J.; Shelhamer, E.; and Darrell, T. 2015. Fully convolutional networks for semantic segmentation. In *The IEEE Conference on Computer Vision and Pattern Recognition*.
- Luc, P.; Couprie, C.; Chintala, S.; and Verbeek, J. 2016. Semantic segmentation using adversarial networks. *arXiv preprint arXiv:1611.08408*.
- Luc, P.; Neverova, N.; Couprie, C.; Verbeek, J.; and LeCun, Y. 2017. Predicting Deeper into the Future of Semantic Segmentation, (code: <https://github.com/facebookresearch/SegmPred>). In *ICCV*.
- Mathieu, M.; Couprie, C.; and LeCun, Y. 2015. Deep multi-scale video prediction beyond mean square error. *arXiv preprint arXiv:1511.05440*.
- Miller, J., and Hardt, M. 2018. When recurrent models don't need to be recurrent. *arXiv preprint arXiv:1805.10369*.
- Morris, V. 2005. Total sky imager (tsi) handbook. *Handbook*.
- Olah, C., and Carter, S. 2016. Attention and augmented recurrent neural networks. *Distill*.
- Paoli, C.; Voyant, C.; Muselli, M.; and Nivet, M.-L. 2010. Forecasting of preprocessed daily solar radiation time series using neural networks. *Solar Energy*.
- Patraucean, V.; Handa, A.; and Cipolla, R. 2015. Spatio-temporal video autoencoder with differentiable memory. *arXiv preprint arXiv:1511.06309*.
- Piergiovanni, A.; Fan, C.; and Ryoo, M. S. 2017. Learning latent sub-events in activity videos using temporal attention filters. In *Thirty-First AAAI Conference on Artificial Intelligence*.
- Ren, M., and Zemel, R. S. 2016. End-to-end instance segmentation and counting with recurrent attention. *arXiv preprint arXiv:1605.09410*.
- Romera-Paredes, B., and Torr, P. H. S. 2016. Recurrent instance segmentation. In *European Conference on Computer Vision*. Springer.
- Seguí, S.; Pujol, O.; and Vitria, J. 2015. Learning to count with deep object features. In *Proceedings of the IEEE Conference on Computer Vision and Pattern Recognition Workshops*.
- Shi, X.; Chen, Z.; Wang, H.; Yeung, D.-Y.; Wong, W.-k.; and Woo, W.-c. 2015. Convolutional lstm network: A machine learning approach for precipitation nowcasting. In *Proceedings of the 28th International Conference on Neural Information Processing Systems, NIPS'15*.
- Srivastava, N.; Mansimov, E.; and Salakhudinov, R. 2015. Unsupervised learning of video representations using lstms. In *International Conference on Machine Learning*.
- Tran, D.; Bourdev, L.; Fergus, R.; Torresani, L.; and Paluri, M. 2015. Learning spatiotemporal features with 3d convolutional networks. In *Proceedings of the IEEE International Conference on Computer Vision*.
- Venugopalan, S.; Xu, H.; Donahue, J.; Rohrbach, M.; Mooney, R.; and Saenko, K. 2014. Translating videos to natural language using deep recurrent neural networks. *arXiv preprint arXiv:1412.4729*.
- Vondrick, C.; Pirsivash, H.; and Torralba, A. 2015. Anticipating the future by watching unlabeled video. *arXiv preprint arXiv:1504.08023*.
- Weinzaepfel, P.; Revaud, J.; Harchaoui, Z.; and Schmid, C. 2013. Deepflow: Large displacement optical flow with deep matching. In *Proceedings of the IEEE International Conference on Computer Vision*.
- Yao, L.; Torabi, A.; Cho, K.; Ballas, N.; Pal, C.; Larochelle, H.; and Courville, A. 2015. Describing videos by exploiting temporal structure. In *Proceedings of the IEEE International Conference on Computer Vision*.
- Yu, F., and Koltun, V. 2015. Multi-scale context aggregation by dilated convolutions. *arXiv preprint arXiv:1511.07122*.
- Zeng, K.-H.; Chen, T.-H.; Chuang, C.-Y.; Liao, Y.-H.; Nibbles, J. C.; and Sun, M. 2017. Leveraging video descriptions to learn video question answering. In *AAAI*, 4334–4340.

Future frame semantic segmentation of time-lapsed videos with large temporal displacement

Supplementary

Summary: We present a novel attention+ConvLSTM based future-frame prediction method with a dual objective over two related tasks on time-lapsed videos: *Segment*: Semantic segmentation mask prediction for next n future frames. *Measure*: Predict n future values of an additional property of each frame.

A large publicly available, semantic segmentation dataset is presented with practical application in alternate energy domain. Our approach outperforms state-of-art by 10.8% for 10 mins (21% over 60 mins) ahead of time predictions, while maintaining a 10.51% nMAE on measure task. Our proposed spatial attention model improves the performance by 3.76% for 10 mins ahead compared to mean attention models.

The sky-videos are accompanied by two ground truth measurements. The semantic masks are obtained from the TSI imager over a calibrated mirror with a robotic arm. This is a specialized instrument that processes the input feed from the mirror (Andreas 1981). The *measure* task ground truth is obtained from a separate pyranometer sensor. Both measurements are continuously streamed on a public website from Colorado, USA.

Model architectural details

The model architecture details are presented here:

- The RGB input image of size $(320, 320, 3)$ is first passed through a ResNet50 Architecture (Yu and Koltun 2015) with kernel regulariser set as l_2 -norm, weight decay of $5e-5$, and batch momentum of 0.9 throughout.
- The resulting vector is then forwarded to an Atrous block with output size $(20, 20, 4)$. This is referred to as the representation vector I in the Architecture Section. We use bilinear upsampling to produce semantic segmentation of $(320, 320, 4)$ corresponding to the 4 classes.
- For *measure*, the same output from the Atrous block is passed through 2 blocks of Conv2D layer with 128 filters of kernel size $(3, 3)$, kernel regulariser set as l_2 -norm and weight decay of $5e-5$ followed by BatchNorm and ReLU activation. The resultant vector of size $(16, 16, 128)$ is flattened and densely connected to 1 unit *measure* prediction output with 0.5 Dropout. The intuition is explained in Model Section.

- For forecasting, all experiments are performed with a look back (t) and forward predict of 6 frames (corresponding to 1 hour). For each consecutive video frames set, 6 representation vectors (\mathbb{I}) corresponding to the 6 input frames are obtained.
- The three-tier ConvLSTM architecture is used to predict the representations of the next 6 frames of size $(6, 20, 20, 4)$. The forecasting architecture consists of three blocks of ConvLSTM2D with 128, 64, and 64 filters respectively each with filter size $(5, 5)$. The ConvLSTM2D layers are alternated with BatchNorm and the output is reshaped to $(6, 20, 20, 4)$ using a Conv3D layer with 4 filters of kernel size $(1, 5, 5)$. The remaining attention vectors are also scaled similarly.

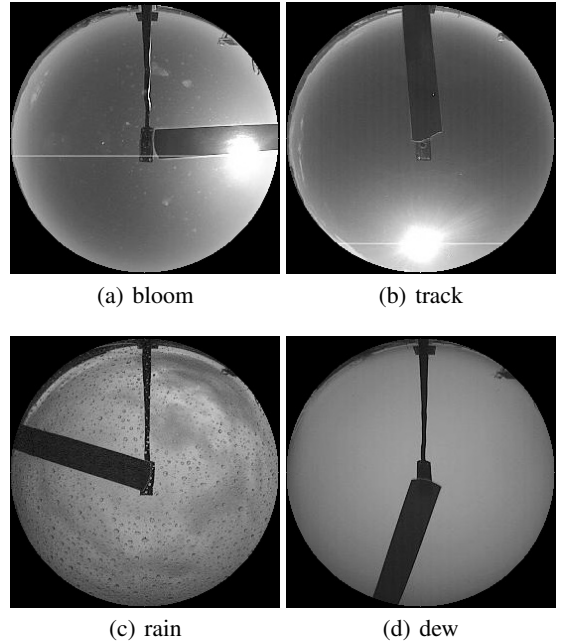


Figure 1: Challenging sky-video frames from the dataset. (a) Blooming effect of bright sun over the occluder, (b) miss-aligned occluder, (c) heavy rain and droplets, (d) dew on the lens after sunrise.

Table 1: Forecasting Architecture with Spatial Attention. # of Parameter : 27,890,703

Layer Type	Output shape	# of Parameters	Connected to
Input_Image	(None, 6, 320, 320, 3)	0	-
TimeDistributed_Vision	(None, 6, 20, 20, 4)	23,595,908	Input_Image
Lambda_Only_Cloud_Dimension	(None, 6, 20, 20)	0	TimeDistributed_Vision
Permute	(None, 20, 20, 6)	0	Lambda_Only_Cloud_Dimension
ConvLSTM_Attention	(None, 20, 20, 64)	416,256	Permute
BatchNorm_1	(None, 20, 20, 64)	256	Conv2D_Attention
Dense_Attention	(None, 20, 20, 6)	390	BatchNorm_1
Reshape	(None, 20, 20, 1, 6)	0	Dense_Attention
Lambda_Replicate_All_Dimension	(None, 20, 20, 4, 6)	0	Reshape
Permute_Attention_Vector	(None, 6, 20, 20, 4)	0	(None, 6, 20, 20, 4)
Attention_Multiply	(None, 6, 20, 20, 4)	0	TimeDistributed_Vision * Permute_Attention_Vector
ConvLSTM_1	(None, 6, 20, 20, 128)	1,690,112	Attention_Multiply
BatchNorm_2	(None, 6, 20, 20, 128)	512	ConvLSTM_1
ConvLSTM_2	(None, 6, 20, 20, 64)	1,229,056	BatchNorm_2
BatchNorm_3	(None, 6, 20, 20, 64)	256	ConvLSTM_2
ConvLSTM_3	(None, 6, 20, 20, 64)	819,456	BatchNorm_3
BatchNorm_4	(None, 6, 20, 20, 64)	256	ConvLSTM_3
Conv3D(f.c. layer)	(None, 6, 20, 20, 4)	6,404	BatchNorm_4
Segment (Bilinear Upsampling)	(None, 6, 320, 320, 4)	0	Conv3D
Conv2D_1	(None, 6, 18, 18, 128)	4,736	Conv3D
BatchNorm_5	(None, 6, 18, 18, 128)	512	Conv2D_1
Activation_ReLu_1	(None, 6, 18, 18, 128)	0	BatchNorm_5
Conv2D_2	(None, 6, 16, 16, 128)	147,584	BatchNorm_5
BatchNorm_6	(None, 6, 16, 16, 128)	512	Conv2D_2
Activation_ReLu_2	(None, 6, 16, 16, 128)	0	BatchNorm_6
Flatten	(None, 6, 32768)	0	Activation_ReLu
Dropout (0.5)	(None, 6, 32768)	0	Flatten
Dense_Measure	(None, 6, 1)	32,769	Dropout (0.5)

Table 2: Spatial Attention (conv2D) pipline. Reduces # of Parameters of the entire model to 27,484,111

Layer Type	Output shape	# of Parameters	Connected to
Conv2D_Attention	(None, 20, 20, 64)	9,664	Permute
BatchNorm_1	(None, 20, 20, 64)	256	Conv2D_Attention
Dense_Attention	(None, 20, 20, 6)	390	BatchNorm_1
Reshape	(None, 20, 20, 1, 6)	0	Dense_Attention
Lambda_Replicate_All_Dimension	(None, 20, 20, 4, 6)	0	Reshape
Permute_Attention_Vector	(None, 6, 20, 20, 4)	0	(None, 6, 20, 20, 4)
Attention_Multiply	(None, 6, 20, 20, 4)	0	TimeDistributed_Vision * Permute_Attention_Vector

- The forecasted representation vector I for each time step can be resolved into *segment* and *measure* as described above.
- The performance of the three-tier ConvLSTM is improved with attention multipliers over the input representation set (II). The multipliers spatially and temporally (element-wise) weights the input vector, and hence is of the same size.
- To produce an attention multiplier of size (6, 20, 20, 4), we first select only the cloud segment of size (6, 20, 20, 1). For spatial attention multiplier, Conv2D of 64 filters with size (5, 5) is applied with BatchNorm over the *temporal* dimension. It is then densely down-sampled to number of samples (6) with *softmax*. This provides a bounded attention value (0-1) over the look back period (6) constrained spatially.
- The attention obtained from the cloud segment channel is replicated to all segmentation classes. Figure 2 illustrates a sample attention mask over laid on the original frames obtained from the spatial attention model described above.
- While we perform experiments on several variations of this architecture in the empirical evaluation, these experiments on architecture search are not exhaustive. However, it is our understanding that the model sufficiently outperforms several satellite based meteorological techniques for solar energy prediction currently in use today.
- Table 3 lists some of the salient properties of the sky-video dataset. The sky-video dataset is larger and has a wider temporal gap as compared to other publicly available datasets. Some challenging frames from the dataset are illustrated in Fig. 1.

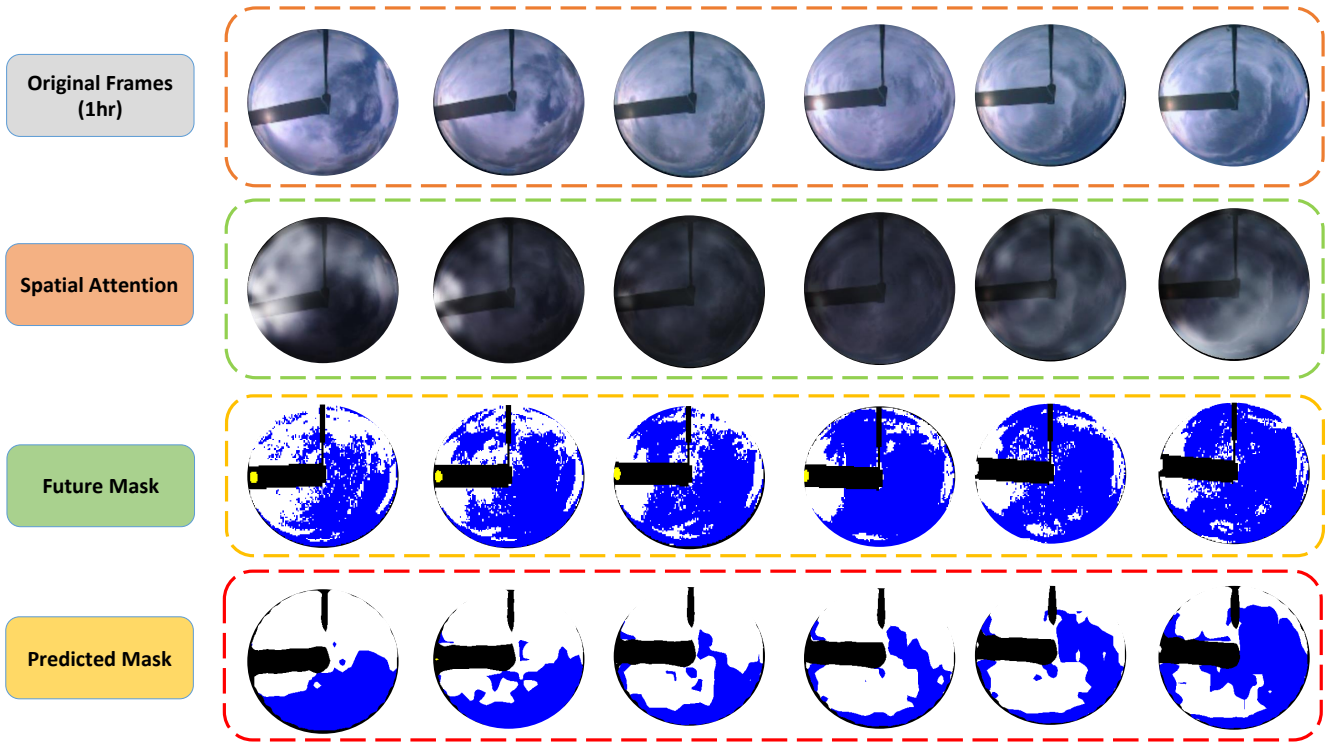


Figure 2: : Performance of *segment* task on a challenging set of six consecutive sequence of frames representing one hour. The illustration contains input, attention-overlay, target, and predicted sequences.

Table 3: Salient properties of Sky-video dataset

Properties	Sky-video
# of train/val	73,120/49,944
total size	123,064
frame rate	6 frames/hour
ground truth	every frame
# of classes	4

Related work in weather prediction

The earliest methods for weather prediction were geometry based models with strong assumptions on functional dependency of position, time and location (Reno, Hansen, and Stein 2012). Highly accurate weather prediction models that are based on coarse grained simulation of physical weather systems are predominantly used in weather prediction (www.ecmwf.int ; www.ncdc.noaa.gov). However, such complex systems have a systematic bias to certain location, time, weather phenomenon, or unpredictable weather occurrences. Recently, several ensemble based techniques have been introduced, that combine physics models with numerical and purely data driven models to fine-tune predictions (Lu et al. 2015). While such approaches show substantial improvement in forecast accuracy, they are limited by the availability of satellite data (typical satellite sweeps range between 3-12hrs), need for enormous computational infrastructure and inability to perform short-term corrections

to predictions. Certain weather parameters can be predicted in short-term horizons with suitable local sensor deployment in a region. Solar-irradiance is one such measure that can be sensed with varying degrees of accuracies. Achleitner (Achleitner et al. 2014) present a approach to aggregate several small photo-sensors for predicting irradiance. While Aryaputera (Aryaputera et al. 2015) present a regression approach to extrapolate weather information to unknown locations. Su (Su et al. 2015) present a local feature approach to explicitly segment and track each cloud with a adaptive gaussian mixture model approach, followed by hand-crafted features for matching clouds across frames for tracking. Other pixel clustering and segmentation based approaches (Wacker et al. 2015; Heinle, Macke, and Srivastav 2010) explicitly measure the cloud cover from sky-images in terms of meteorological unit of *okta* (the number of eighths of the sky occluded by clouds) and cloud type.

References

- [Achleitner et al. 2014] Achleitner, S.; Kamthe, A.; Liu, T.; and Cerpa, A. E. 2014. Sips: Solar irradiance prediction system. In *Proceedings of the 13th International Symposium on Information Processing in Sensor Networks*. IEEE Press.
- [Andreas 1981] Andreas, A.; Stoffel, T. 1981. Nrel solar radiation research laboratory (srll): Baseline measurement system (bms).
- [Aryaputera et al. 2015] Aryaputera, A. W.; Yang, D.; Zhao, L.; and Walsh, W. M. 2015. Very short-term irradiance forecasting at unobserved locations using spatio-temporal kriging. *Solar Energy*.
- [Heinle, Macke, and Srivastav 2010] Heinle, A.; Macke, A.; and Srivastav, A. 2010. Automatic cloud classification of whole sky images. *Atmospheric Measurement Techniques*.
- [Lu et al. 2015] Lu, S.; Hwang, Y.; Khabibrakhmanov, I.; Mariano, F. J.; Shao, X.; Zhang, J.; Hodge, B.-M.; and Hamann, H. F. 2015. Machine learning based multi-physical-model blending for enhancing renewable energy forecast-improvement via situation dependent error correction. In *Control Conference (ECC), 2015 European*. IEEE.
- [Reno, Hansen, and Stein 2012] Reno, M. J.; Hansen, C. W.; and Stein, J. S. 2012. Global horizontal irradiance clear sky models: Implementation and analysis. *Tech. Report*.
- [Su et al. 2015] Su, F.; Jiang, W.; Zhang, J.; Wang, H.; and Zhang, M. 2015. A local features-based approach to all-sky image prediction. *IBM Journal of Research and Development*.
- [Wacker et al. 2015] Wacker, S.; Gröbner, J.; Zysset, C.; Diener, L.; Tzoumanikas, P.; Kazantzidis, A.; Vuilleumier, L.; Stöckli, R.; Nyeki, S.; and Kämpfer, N. 2015. Cloud observations in Switzerland using hemispherical sky cameras. *Journal of Geophysical Research: Atmospheres*.
- [www.ecmwf.int] www.ecmwf.int. European centre for medium-range weather forecasts.
- [www.ncdc.noaa.gov] www.ncdc.noaa.gov. National centers for environmental prediction.
- [Yu and Koltun 2015] Yu, F., and Koltun, V. 2015. Multi-scale context aggregation by dilated convolutions. *arXiv preprint arXiv:1511.07122*.